Solid State Ionics 181 (2010) 1473–1477

Contents lists available at ScienceDirect

Solid State Ionics

journal homepage: www.elsevier.com/locate/ssi

The origin of elastic anomalies in thin films of oxygen deficient ceria, CeO_{2-x}

Anna Kossoy [a], Anatoly I. Frenkel [b], Yishay Feldman [c], Ellen Wachtel [c], Alla Milner [a], Igor Lubomirsky [a,*]

[a] Dept. of Materials and Interfaces, Weizmann Institute of Science, Rehovot, 76100, Israel
[b] Dept. of Physics, Yeshiva University, New York, NY 10016, USA
[c] Chemical Research Support Unit, Weizmann Institute of Science, Rehovot, 76100, Israel

ARTICLE INFO

Article history:
Received 19 April 2010
Received in revised form 31 August 2010
Accepted 1 September 2010

Keywords:
Gadolinium-doped ceria
Chemical strain
Elasticity
Extended X-ray absorption fine structure spectroscopy (EXAFS)
Thermal expansion

ABSTRACT

Self-supported films of $CeO_{1.95}$ display time-scale dependent elastic moduli, a phenomenon which has been termed the chemical strain effect. In order to probe the possible structural origins of this behavior, extended X-ray absorption fine structure spectroscopy and X-ray diffraction were used. Evidence was found that, although this oxygen deficient ceria appears to maintain the fluorite structure on average, the mean *Ce–O* bond length is shorter than the mean Ce–oxygen vacancy distance. This finding is consistent with crystallographic data from more strongly reduced ceria in which the oxygen vacancies are ordered. By studying strain induced structural changes, we show that it is possible to relate this lattice distortion to the chemical strain effect. Similar conclusions were previously reached for films of $Ce_{0.8}Gd_{0.2}O_{1.9}$. Since the ionic radii of both Gd^{3+} and Ce^{3+} are larger than that of Ce^{4+}, we suggest that when cation dopants are larger than the host, ceria compounds containing a high concentration of oxygen vacancies may exhibit elastic anomalies.

1. Introduction

Thin films of $Ce_{0.8}Gd_{0.2}O_{1.9}$, one of the most important ionic conductors [2–5], exhibit a number of elastic anomalies, i.e. both spontaneous changes in the lattice parameters as well as inelastic effects. The most striking of these is the ability to exhibit two different elastic moduli depending on time-scale [1,6]. This phenomenon, which has been called the chemical strain effect [6], can cause an absolute change in volume of ~0.2% even if the external stress is homogeneous [1]. As such, the internal reorganization of point defects has been cited as a probable cause of the inelastic behavior (chemical strain) rather than the more commonly observed stress gradient-induced diffusion [7]. Recently, the local bonding in $Ce_{0.8}Gd_{0.2}O_{1.9}$ was studied by extended X-ray absorption fine structure (EXAFS) spectroscopy [8]. This work revealed that in $Ce_{0.8}Gd_{0.2}O_{1.9}$, the cation–O bond is shorter than would be expected on the basis of the X-ray diffraction measurements of the average fluorite structure. Analyses of the 1st and 2nd coordination shells of Ce and Gd provided evidence that (1) the average distance from a Ce ion to an oxygen vacancy is larger than the mean *Ce–O* bond length and that (2) supported the theoretical finding that oxygen vacancies induced by Gd-doping prefer coordination with Ce ions rather than with Gd ions [9]. Furthermore, it was found that in the presence of compressive strain of $0.3 \pm 0.1\%$, the average *Ce–O* bond length is decreased by $1 \pm 0.5\%$. The rearrangement of the *Ce–O* bond under strain was cited as a probable cause of the elastic anomalies in $Ce_{0.8}Gd_{0.2}O_{1.9}$.

The fact that it is the host cation, Ce^{4+}, that is involved in producing elastic anomalies led to the hypothesis that even pure ceria, if it contains a large amount of oxygen vacancies, should display similar local lattice distortion and, as a result, similar elastic anomalies. To test this concept, we compared the *Ce–O* bond lengths deduced either from EXAFS or X-ray diffraction (XRD) for oxygen deficient ceria films (CeO_{2-x}). Our data demonstrate that although oxygen deficiency results in an increase in the dimension of the fluorite unit cell of CeO_{2-x} as measured by XRD, the average Ce–O bond length contracts. In addition, we have indeed found evidence of elastic anomalies in thin, self-supported films of CeO_{2-x}, which are similar to those previously observed in thin films of $Ce_{0.8}Gd_{0.2}O_{1.9}$ [1,6,10].

2. Experimental

Substrate-supported 400 ± 20 nm thick films of CeO_{2-x} were prepared by radio frequency magnetron plasma sputtering at room temperature from a stoichiometric CeO_2 target (Semiconductor Materials, 99.95) onto (001) Si 275 ± 25 μm thick wafers [10,11] with pure Ar as a sputtering gas. The film thickness (400 ± 20 nm) was chosen such that the substrate supported films were thin enough that they did not undergo delamination (below critical thickness), while the self-supported films, described below, could retain structural integrity. Following the deposition, the substrate-supported films were annealed in air for 10 h at 400 °C or 550 °C. The heating rate was 10 °C/min and the cooling rate, 1 °C/min. The X-ray diffraction (XRD) patterns of the substrate-supported films were

* Corresponding author. Tel.: +972 8 9342142.
E-mail addresses: Anatoly.Frenkel@yu.edu (A.I. Frenkel), Igor.Lubomirsky@weizmann.ac.il (I. Lubomirsky).

0167-2738/$ – see front matter © 2010 Elsevier B.V. All rights reserved.
doi:10.1016/j.ssi.2010.09.001

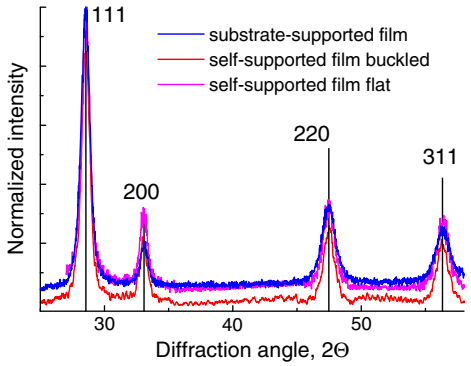

Fig. 1. XRD patterns of $CeO_{1.95}$ films: substrate supported; self-supported (not exposed to oxygen plasma) buckled and flat. The diffraction pattern of the flat film was acquired after heating to 150 °C. No differences in the peak positions are observed.

acquired with a Rigaku TTRAXIII diffractometer (Cu K_α radiation) operating in the Bragg–Brentano (θ–2θ) mode with 3° theta offset to avoid the silicon λ/2 reflection at 2θ≈32°. The peak positions were determined relative to the LaB_6 reference by fitting the peak profile to a pseudo-Voigt function and subtracting the $K_{\alpha 2}$ contribution. To determine the lattice parameter of the films, the position of the (422) diffraction peak was measured with a slow scan rate (0.01°/min). The accuracy of the determination of the unit cell size for diffraction angles 2θ>80° was ±0.002 Å. The crystallite size of the CeO_{2-x} films was determined from the width of the XRD peaks and was close to the grain size determined from images acquired by scanning electron microscopy (LEO Ultra55) with pattern recognition software. The stress in the substrate-supported films was deduced from changes in the substrate curvature (accuracy 1/1200 m) [12,13]. Coarse grained powders were obtained from the stoichiometric CeO_2 target.

After annealing, some of the substrate-supported films were converted into circular 100–150 μm diameter self-supported tethered films by local substrate removal with SF_6-based deep reactive ion etching. The films annealed at 550 °C were etched with oxygen in the plasma at the final stage to ensure that they remained saturated with oxygen. The films annealed at 400 °C were etched without oxygen in the plasma to prevent further oxidation. Self-supported films were subjected to heating and cooling in the atomic force microscope NT-MDT similar to the process described in Ref. [6]. Flattening time of the buckled films was measured from the same initial height. The XRD patterns of self-supported films were measured in the transmission mode through the etched region in the Si substrate, so that only the signal from the self-supported region was collected. Their analysis was performed as described above.

Raman spectroscopy measurements of the self-supported and substrate supported films were performed with a Micro-spot Renishaw Raman spectrometer with excitation wavelength of 633 nm. The average length of the *Ce–O* bond was deduced from the EXAFS data on the substrate-supported films, following annealing either at 400 °C or 550 °C. The protocol for the Ce L_{III} EXAFS measurements performed on beamlines X18B and X19A at the National Synchrotron Light Source, Brookhaven National Laboratory was the same as that described in Ref. [8]. Bond lengths were determined with the IFEFFIT data analysis package (Ref. [8,14]). For all R-space fitting with FEFF6, k^3-weighting and the k-range from 2 to 9.5 $Å^{-1}$ were used. No Fourier transform filtering was performed. Fitting of the 2nd nearest neighbor distance in CeO_2 is strongly perturbed by multi-electron excitations and multiple-scattering due to collinear three-atom linkages [15]. Therefore only the 1st cation coordination shell was fitted, and the R-window for the fit was chosen between ca. 1.8 and 3 Å, depending on the sample. The coordination number of Ce-cation pairs was fixed at 8 for all films.

3. Results and analysis

3.1. Stress and strain in thin films of CeO_{2-x}

According to XRD data, both self-supported and substrate-supported films were crystalline and appear to be in the fluorite phase (Fig. 1). The as-deposited substrate-supported films of CeO_{2-x} were under compressive stress of 200–800 MPa. The presence of compressive stress correlated with the presence of in-plane compressive strain of ≈1.00±0.05%, deduced from the dependence of the position of the (422) X-ray diffraction peak on the inclination angle. The position of this peak was also used to estimate the oxygen content in the films using the relationship between the lattice parameter and the stoichiometry given in Ref. [3]. The oxygen content of the as-deposited substrate-supported films can only be estimated approximately due to the presence of compressive strain: 1.90±0.02% (henceforth $CeO_{1.90}$ films). The stress and strain in substrate-supported films following annealing in air at 400 °C were below the detection limits (strain <0.04% and stress <30 MPa). The oxygen content of these films was estimated to be 1.95±0.01 (unit cell size 5.435±0.002 Å). These films are henceforth termed $CeO_{1.95}$. For the substrate-supported films annealed at 550 °C the unit cell size was 5.414±0.002 [16], which is close to that of stoichiometric ceria (henceforth CeO_2 films). The SEM-derived grain size of all films was within the range 20–45 nm (85% by volume). The self-supported films prepared from the substrate supported $CeO_{1.95}$ films expanded and buckled (Fig. 2a), adopting a dome-like shape immediately upon removal of the substrate. The degree of expansion (film-window misfit strain) was determined by the shift in the microscope focus and is equal to $u_{mf}=0.045\pm0.01\%$, which is slightly above the upper limit for the buckling threshold for these films ≈0.035%. (It should be noted that the buckling strain is independent of the elastic modulus [17].) This value is close to the uncertainty of the XRD-based strain measurements. However, according to these data, the relaxed biaxial modulus of the films cannot exceed 30 MPa/u_{mf}=64 GPa, which is much smaller than the biaxial modulus of bulk CeO_2 (236 GPa [3]).

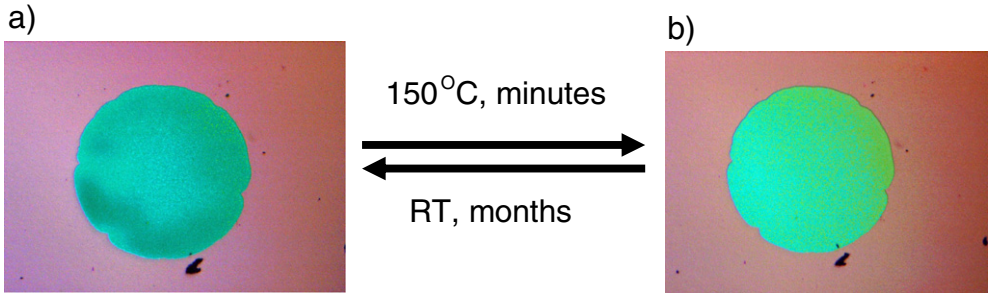

Fig. 2. a) A self-supported film of $CeO_{1.95}$ after etching (not exposed to oxygen plasma); b) the same film after heating to 150 °C for less than 3 min. The flat film reverts to a buckled state after three months of storage in a dry atmosphere at room temperature.

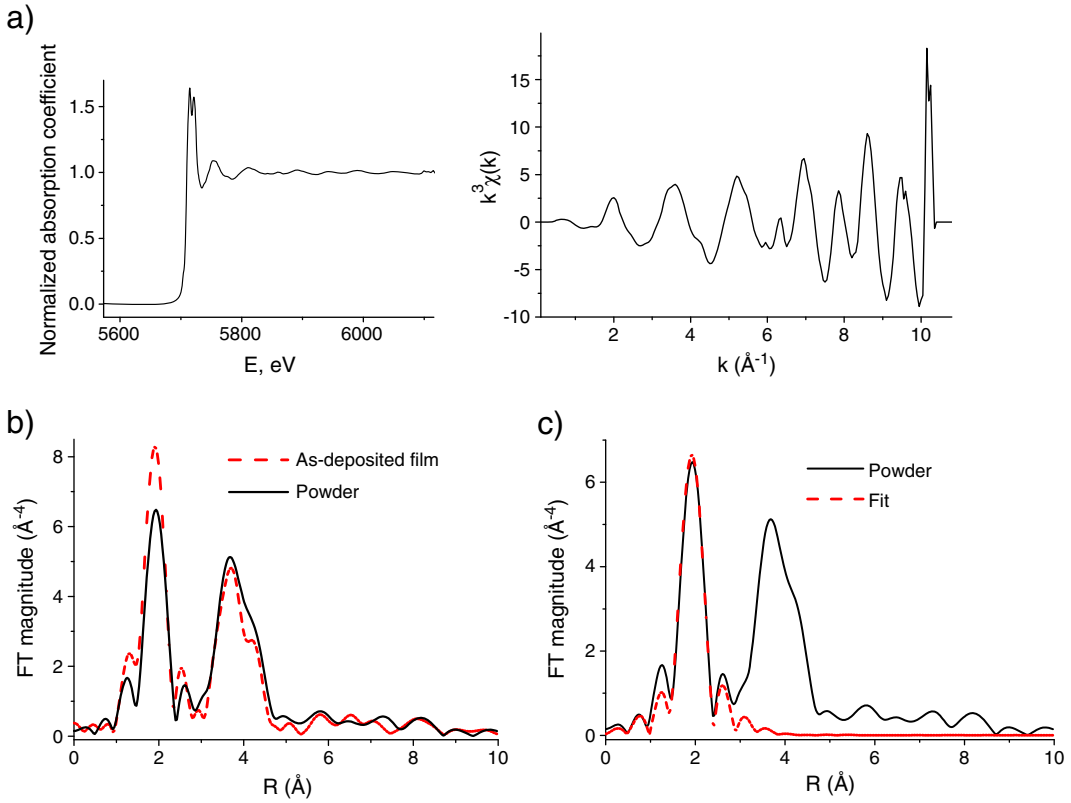

Fig. 3. a) Normalized EXAFS spectra for CeO_2 powder (left) and k^3 weighted fine structure curve (right); b) Fourier transform magnitudes of the Ce L_{III} edge EXAFS spectra of CeO_2 powder and a thin as-deposited film of cerium oxide ($CeO_{1.9}$); c) data and FEFF6 fit for the coarse grain powder spectrum.

3.2. Ce–O bond length in thin films of oxygen deficient ceria

Fig. 3a shows the normalized Ce L_{III} EXAFS spectrum for coarse grained CeO_2 powder, along with the weighted fine structure function, $k^3\chi(k)$. The Fourier transform magnitudes of these data as well as of those for a thin, as-deposited film of $CeO_{1.9}$ are compared in Fig. 3b. For the case of reduced ceria, we note that the EXAFS signal originates from both the Ce^{3+} and Ce^{4+} absorbers, and therefore the spectrum corresponds to the weighted average of both valence states. Fitting FEFF6 theory to the CeO_2 powder data was performed for both the imaginary and real parts of the Fourier-transformed EXAFS spectra and the results are shown in Fig. 3c. The best fit value of the mean *Ce–O* bond length was $L^{EXAFS}_{CeO_2} = 2.340 \pm 0.009$ Å. The same value was found for the thin films of stoichiometric ceria. The EXAFS result also agrees with the *Ce–O* bond length deduced from the XRD measurements of the films (Fig. 4) ($L^{XRD}_{CeO_2} = 2.343 \pm 0.001$ Å), assuming that ionic positions correspond to those of the perfect fluorite structure. The XRD-derived *Ce–O* bond length for the substrate-supported $CeO_{1.95}$ films ($L^{XRD}_{CeO_{1.95}} = 2.353 \pm 0.001$ Å) is significantly larger than that of CeO_2 films $L^{XRD}_{CeO_{1.95}} > L^{XRD}_{CeO_2}$ (Fig. 4) as would be expected [3]. However, the EXAFS-derived average *Ce–O* bond length in the $CeO_{1.95}$ films ($L^{EXAFS}_{CeO_{1.95}} = 2.334 \pm 0.006$ Å) is significantly shorter than that derived from the XRD data. Similarly, the EXAFS-derived average *Ce–O* bond length for the $CeO_{1.90}$ film ($L^{EXAFS}_{CeO_{1.90}} = 2.319 \pm 0.007$ Å) is much shorter than that derived from the XRD data ($L^{XRD}_{CeO_{1.90}} = 2.369 \pm 0.004$ Å).

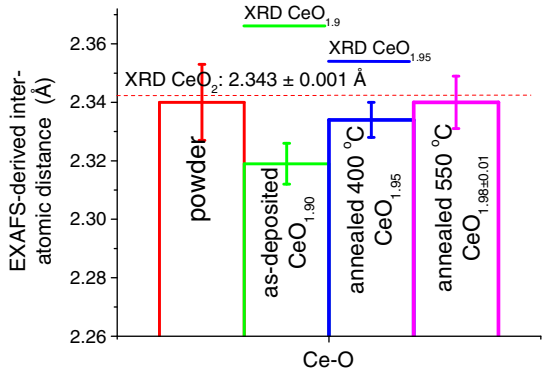

Fig. 4. Comparison of the XRD-derived and EXAFS-derived cation–anion bond lengths obtained for coarse grain powders and thin films of ceria (data from Table 1).

3.3. Inelastic effects in self-supported $CeO_{1.95}$ films

Following substrate removal, the self-supported films prepared from $CeO_{1.95}$ films become buckled. The misfit compressive strain measured from the buckling height and window dimensions is $u_{mf} = 0.045 \pm 0.01\%$. However, upon heating to 150–200 °C for a few minutes (see Fig. 2), the films flatten and remain flat upon slow cooling (<2 °C/min), maintaining their mechanical integrity. Three months storage at room temperature is sufficient to restore them to their initial buckled state (Fig. 2b). This cycle can then be repeated:

Table 1
Fitting results for the 1st coordination shell of Ce in ceria films and powders.

Sample	Composition	*Ce–O* distance from XRD, Å	Lattice parameter, Å	*Ce–O* distance obtained from EXAFS, Å
Powder	CeO_2	2.343 ± 0.001	5.411	2.340 ± 0.013
As-deposited film	$CeO_{1.90}$	2.366 ± 0.002	5.465	2.319 ± 0.007
Film annealed at 400 °C	$CeO_{1.95}$	2.354 ± 0.002	5.437	2.334 ± 0.006
Film annealed at 550 °C	CeO_2	2.344 ± 0.002	5.413	2.340 ± 0.009

heating–flattening–storage–spontaneous restoration of the buckled state. As a control, we observed that the self-supported films of CeO_2 do not buckle upon substrate removal but rather display a linear thermal expansion coefficient $\gamma = 8.3 \cdot 10^{-6}\,K^{-1}$ upon heating between 70 °C and 130 °C (Fig. 5). They are buckled only as long as they are kept at the elevated temperature. During subsequent storage at room temperature, they remain flat and do not exhibit elastic anomalies. These data for the CeO_2 films confirm that the room temperature behavior of the $CeO_{1.95}$ films cannot be attributed to oxygen loss, since below 300 °C in air, loss of oxygen is not expected to take place [18,19].

From the dependence of the time of flattening from a given height (h) of the self-supported $CeO_{1.95}$ films versus the inverse of the temperature to which they are heated, one can deduce [1] that the activation energy of the process responsible for the volume reduction is 1.2 ± 0.2 eV (Fig. 6). This is very close to the value observed for the self-supported $Ce_{0.8}Gd_{0.2}O_{1.9}$ films [1]. Furthermore, if a self-supported $CeO_{1.95}$ film in the "flat" state at room temperature is subjected to rapid heating (>10 °C/s) to a temperature T (150–200 °C), it becomes buckled, a state which lasts for a few tens of seconds. The height of buckling, h, produced by the rapid heating, follows $h^2 \propto T - T_{buckling}$ (cf. Fig. 3 in Ref. [6]). After a few tens of seconds in the buckled state the films flatten. As described above, upon slow cooling (<2 °C/min) from 150 to 200 °C, the self-supported $CeO_{1.95}$ films remain flat and retain mechanical integrity; however, sufficiently rapid cooling (>10 °C/min), causes film disintegration. Also in this regard, the behavior of the self-supported $CeO_{1.95}$ films is analogous to that of the self-supported films of $Ce_{0.8}Gd_{0.2}O_{1.9}$ described in Refs. [1,6,10].

We note that the expansion described above cannot be attributed to uptake/loss of water because: (1) X-ray photoelectron spectroscopy does not detect changes in water content; (2) significantly higher temperatures (>350 °C) are necessary to cause water desorption from the ceria surface [18]. The expansion also cannot be attributed to a major structural modification because the Raman spectra presented in Fig. 7 do not show any changes in the F_{2g} line, which is sensitive to phase transitions in oxygen deficient ceria [20].

4. Discussion

CeO_{2-x} is known to expand upon reduction [3], with the fluorite lattice constant displaying a linear increase between x = 0–0.1, as would be predicted by Vegard's law. This increase has been attributed to the difference in atomic radii of the Ce^{3+} and Ce^{4+} ions and/or the difference in the volume of the oxygen vacancy as compared to that of the oxide ion. That Vegard's law is obeyed even in the presence of a phase change, leaves open the question of whether or not CeO_{2-x} can be regarded as a simple solid solution of Ce_2O_3 in CeO_2. Nevertheless, the expansion of the ceria lattice upon reduction implies that the average cation–anion distance, as calculated from diffraction data, must also increase. However, as detailed above, using EXAFS to study local bonding distances shows that in $CeO_{1.95}$ the average Ce–O distance ($L^{EXAFS}_{CeO_{1.95}}$) is in fact smaller than the XRD-derived cation–anion distance ($L^{XRD}_{CeO_{1.95}}$). One would expect that for a single phase material, the average first nearest neighbor bond length would be close to the XRD-derived values. The observed difference may be attributed to the presence of 2.5% oxygen vacancies which do not contribute to the EXAFS-derived cation–oxygen distances but do affect the XRD-derived average first nearest neighbor distance. If we assume a perfect fluorite lattice with randomly distributed oxygen vacancies, and follow Ref. [21], it is possible to estimate the average cation–vacancy distances, as

$$\overline{L_{Ce\text{–}Vac,CeO_{1.95}}} = \left(L^{XRD}_{CeO_{1.95}} - (1.95/2)\cdot L^{EXAFS}_{CeO_{1.95}}\right) / (1 - 1.95/2) = 3.10 \pm 0.28\,\text{Å} \quad (1)$$

and

$$\overline{L_{Ce\text{–}Vac,CeO_{1.9}}} = \left(L^{XRD}_{CeO_{1.9}} - (1.9/2)\cdot L^{EXAFS}_{CeO_{1.9}}\right) / (1 - 1.9/2) = 3.32 \pm 0.26\,\text{Å} \quad (2)$$

The values of the displacements inferred from Eqs. (1) and (2) are unreasonably large, particularly in view of the ionic radii

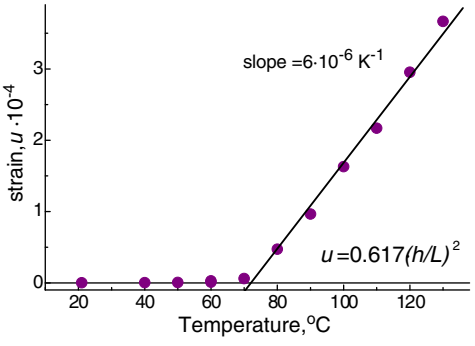

Fig. 5. Determination of the thermal expansion coefficient of a self-supported CeO_2 film. The film-window strain, u, was calculated from the buckling height, h (measured by AFM), and film diameter, $2L$, as a function of temperature. The difference between the thermal expansion coefficient of the film and that of the Si window $\Delta\gamma = 6 \cdot 10^{-6}\,K^{-1}$ is determined from the linear slope in the temperature range above 70 °C. According to this measurement the thermal expansion coefficient of the film is $\gamma(CeO_2) = \Delta\gamma + \gamma(Si) = 8.3 \cdot 10^{-6}\,K^{-1}$, which is smaller than for bulk CeO_2 ($11–12 \cdot 10^{-6}\,K^{-1}$) but close to that obtained for self supported films of $Ce_{0.8}Gd_{0.2}O_{1.9}$ [1].

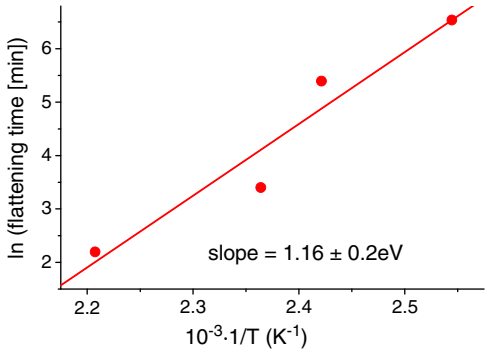

Fig. 6. Semi-logarithmic plot of the time of flattening of a self-supported $CeO_{1.95}$ film (400 nm thick) as a function of the inverse temperature.

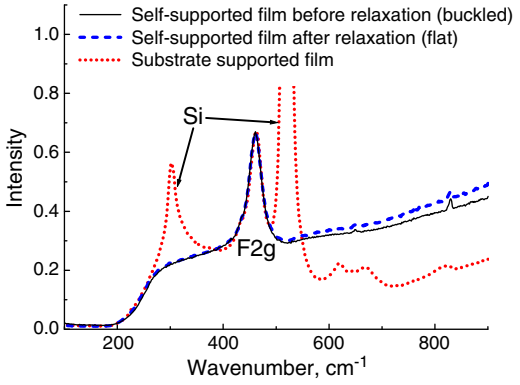

Fig. 7. Representative Raman spectra of a $CeO_{1.95}$ substrate-supported film annealed at 400 °C and flat/buckled self-supported films of the same sample. No significant changes in the F_{2g} peak are observed, indicating absence of major structural changes.

$r_{Ce^{4+}}^{CN=8} = 1.11$ Å, $r_{Ce^{3+}}^{CN=8} = 1.28$ Å and $r_{O^{2-}}^{CN=4} = 1.24$ Å [22]. Therefore we must conclude that, given the absence of crystallographic data for $CeO_{1.9}$ and $CeO_{1.95}$, our assumption of perfect fluorite symmetry for the films of reduced ceria cannot be correct. This is consistent with the fact that any deviation of the anion sub-lattice from the fluorite structure would not be readily detectable by XRD since the atomic structure factor of oxygen is less than 1/6 that of Ce and the largest contribution of oxygen ions to the amplitude of the XRD peaks does not exceed 24% (220 and 200 peaks).

It is known that at the stoichiometry of $Ce_{11}O_{20}$ ($CeO_{1.82}$), ceria transforms into a triclinic P-1 phase with ordered oxygen vacancies [23,24], while the powder diffraction pattern remains close to that of a fluorite phase [25]. These crystallographic data show that the tetrahedron of Ce ions surrounding an oxygen vacancy is more expanded than that surrounding an oxygen ion. The four nearest neighbor Ce ions relax outward from the oxygen vacancy by approximately 0.2 Å with respect to the perfect fluorite positions, while the oxygen atoms of the second coordination layer move inwards toward the vacancy by 0.3 Å [24,26] The regions between the empty tetrahedra experience significant compression. Our data are consistent with the presence of such a coordination defect, yet the distance estimates given in Eqs. (1) and (2) must be viewed only as qualitative indicators of the local lattice distortion.

As reported previously, the presence of substrate-imposed compressive strain increases the lattice distortion [8] and therefore, in $CeO_{1.9}$ films, the observed decrease in the *Ce–O* bond length is likely the combined result of both oxygen deficiency and compressive strain. In the case of $Ce_{0.8}Gd_{0.2}O_{1.9}$ [8], EXAFS data were able to show that the average distance from oxygen to the Ce^{4+} host cation decreases when the film is compressed, while the distance from oxygen to the dopant Gd^{3+}, which has the larger ionic radius, $r_{Gd^{3+}}^{CN=8} = 1.19$ Å, $r_{Ce^{4+}}^{CN=8} = 1.11$ Å [22], remains unchanged within the measurement uncertainty. As noted above, EXAFS cannot be used to distinguish the interatomic distances relative to Ce^{3+} from those relative to Ce^{4+}. However, since the ionic radius of Ce^{3+} is even larger than that of Gd^{3+}, we expect that in the case of oxygen deficient ceria, it is only the Ce^{4+} host cations that relax outward from an oxygen vacancy. This supposition is supported by DFT calculations [26] that show that the Ce^{3+} ions are energetically unlikely to be in the first coordination layer of an oxygen vacancy.

We therefore summarize the scenario for the chemical strain effect as follows. Thin films of oxygen deficient ceria display local structural distortions that are quite similar to those observed in $Ce_{0.8}Gd_{0.2}O_{1.9}$. At room temperature, the cations and the anions shift with respect to each other so that Ce ions are observed to move away from the oxygen vacancies, locally distorting the symmetry. The fact that self-supported films of $CeO_{1.95}$ spontaneously buckle at room temperature suggests that this shift of the Ce ions results in an initial volume increase. Heating decreases the repulsion between the Ce^{4+} ions and the oxygen vacancies, thereby restoring the more symmetrical environment and leading to film flattening. The activation energy deduced from the film flattening time is comparable to that measured for the self-supported $Ce_{0.8}Gd_{0.2}O_{1.9}$ films [1]. This suggests that the microscopic processes jointly responsible for local distortions and elastic anomalies are similar for both oxygen deficient and Gd-doped ceria.

We note that the concentration of the oxygen vacancies in $CeO_{1.95}$ is only half of that in $Ce_{0.8}Gd_{0.2}O_{1.9}$. Nevertheless, $CeO_{1.95}$ and $Ce_{0.8}Gd_{0.2}O_{1.9}$ exhibit similar elastic behavior. We suggest that a plausible reason for the proportionally stronger effect in $CeO_{1.95}$ is the fact that the Ce^{3+} ion is significantly larger than Gd^{3+} ($r_{Ce^{3+}}^{CN=8} = 1.28$ Å, $r_{Gd^{3+}}^{CN=8} = 1.19$ Å, $r_{Ce^{4+}}^{CN=8} = 1.11$ Å [22]). Using Rietveld analysis of synchrotron XRD data from a series of doped ceria samples, Yashima and Takizawa [27] showed that the extent of positional disorder, local distortion and resulting lattice strain in doped ceria is indeed systematically related to the size difference between the host Ce^{4+} and the triply ionized dopant cation. We suggest that different onsets of interaction of these local distortions may explain why oxygen deficient ceria loses fluorite symmetry and becomes triclinic [24] already at 9% oxygen vacancies ($CeO_{1.82}$), whereas $Ce_{1-x}Gd_xO_{2-x/2}$ loses macroscopic fluorite symmetry only at $Ce_{1-x}Gd_xO_{2-x/2}$, x = 0.4 ([28]).

5. Conclusions

Combined EXAFS and XRD measurements provide evidence that oxygen deficiency in substrate-supported ceria films results in a decrease in the mean Ce–O bond length and an increase in the average Ce–oxygen vacancy distance. Using crystallographic data for reduced ceria with ordered oxygen vacancies, we interpret these results as being due to expansion of the empty cation tetrahedra which leads to compression in the region of the oxygen containing tetrahedra. A qualitatively similar local distortion was observed in $Ce_{0.8}Gd_{0.2}O_{1.9}$. Self-supported films of oxygen deficient ceria $CeO_{1.95}$ exhibit elastic anomalies with activation energy comparable to that observed in $Ce_{0.8}Gd_{0.2}O_{1.9}$, indicating that the same microscopic mechanism leads to local structural distortion in both cases. These findings also support our previous suggestion [8] that pure and doped ceria compounds containing a large concentration of vacancies will exhibit elastic anomalies when the trivalent cation is larger than Ce^{4+} .

Acknowledgements

I.L. wishes to acknowledge the US–Israel Binational Science Foundation, the Israel Ministry of Science and the Israeli Science Foundation for support. This research is made possible in part by the generosity of the Harold Perlman Family. AIF gratefully acknowledges the support of this work by U.S. DOE Grant No. DE-FG02-03ER15476. The use of the NSLS beamlines was supported by U.S. DOE Contract No. DE-AC02-98CH10886. Beamlines X18B and X19A at the NSLS are supported in part by the Synchrotron Catalysis Consortium, U.S. DOE Grant No. DE-FG02-05ER15688.

References

[1] A. Kossoy, Y. Feldman, R. Korobko, E. Wachtel, I. Lubomirsky, J. Maier, Adv. Func. Mater. 19 (2009) 634.
[2] H. Inaba, H. Tagawa, Sol. State Ionics 83 (1996) 1.
[3] M. Mogensen, N.M. Sammes, G.A. Tompsett, Sol. State Ionics 129 (2000) 63.
[4] H.L. Tuller, Sol. State Ionics 131 (2000) 143.
[5] L.J. Gauckler, D. Beckel, B.E. Buergler, E. Jud, U.R. Muecke, M. Prestat, J.L.M. Rupp, J. Richter, Chimia 58 (2004) 837.
[6] A. Kossoy, Y. Feldman, E. Wachtel, I. Lubomirsky, Adv. Func. Mater. 17 (2007) 2393.
[7] H.W. Hayden, W.G. Moffatt, J. Wulff, The Structure and Properties of Materials, John Wiley & Sons, New York, 1965.
[8] A. Kossoy, A.I. Frenkel, Q. Wang, E. Wachtel, I. Lubomirsky, Adv. Mater. 22 (2010) 1.
[9] M. Nakayama, M. Martin, Phys. Chem. Chem. Phys. 11 (2009) 3241.
[10] M. Greenberg, E. Wachtel, I. Lubomirsky, J. Fleig, J. Maier, Adv. Func. Mater. 16 (2006) 48.
[11] A. Kossoy, Y. Feldman, E. Wachtel, K. Gartsman, I. Lubomirsky, J. Fleig, J. Maier, Phys. Chem. Chem. Phys. 8 (2006) 1111.
[12] G.G. Stoney, Proc. R. Soc. London A82 (1909) 172.
[13] C.A. Volkert, J. Appl. Phys. 70 (1991) 1.
[14] M. Newville, J. Synchrotron Rad. 8 (2001) 322.
[15] E. Fonda, D. Andreatta, P.E. Colavita, G. Vlaic, J. Synchrotron Rad. 6 (1999) 34.
[16] PDF#34-0394, Natl. Bur. Stand. (U.S.) Monogr. 25, 20 38 (1983).
[17] F. Bloom, D. Coffin, Handbook of Thin Plate Buckling and Postbuckling, CHAPMAN & HALL/CRC, London-New York, 2001.
[18] S. Kim, R. Merkle, J. Maier, Surf. Sci. 549 (2004) 196.
[19] S.R. Bishop, K.L. Duncan, E.D. Wachsman, Electrochim. Acta 54 (2009) 1436.
[20] A. Banerji, V. Grover, V. Sathe, S.K. Deba, A.K. Tyagi, Sol. State. Comm. 149 (2009) 1689.
[21] J.C. Mikkelsen, J.B. Boyce, Phys. Rev. Lett. 49 (1982) 1412.
[22] www.webelements.com.
[23] I. Riess, R. Koerner, M. Ricken, J. Noelting, Sol. State Ionics 28 (1988) 539.
[24] E.A. Kummerle, G. Heger, J. Sol. State Chem. 147 (1999) 485.
[25] International Crystallographic Structure Database (ISCD); reference file 88758; $Ce_{11}O_{20}$.
[26] E. Shoko, M.F. Smith, R.H. McKenzie, J. Phys. Condens. Matter 22 (2010).
[27] M. Yashima, T. Takizawa, J. Phys. Chem. C 114 (2010) 2385.
[28] V. Grover, A.K. Tyagi, MRS Bull. 39 (2004) 859.